Design Proposal for a Mach-Zehnder Interferometer

Álvaro J. Lebrun (aj_lebrun) alvaro.lebrun@ipronics.com

***Abstract*—This document describes the design of various Mach-Zehnder interferometers for silicon photonics as well as the simulation of the expected result for each of the interferometers, studying the effect of parameter variations in each interferometer.**

I. INTRODUCTION

THE Mach-Zehnder interferometer (MZI) is a building block in silicon photonics characterized by splitting a beam of light into two paths and then recombining them to produce interference. By changing certain parameters like the length of the paths or the temperature applied to one waveguide using thermo-optical phase shifters, the resulting interference can be modified, allowing numerous possible applications. For example, optical modulation, switching, and sensing, which have made the MZI a very popular device to study. In this document we propose different versions of a Mach-Zehnder interferometer focusing on the variation in length of one of the paths of the interferometer.

II. THEORY

The simplest form of a Mach-Zehnder interferometer consists of one beam-splitter that divides a beam of light into two paths, which have the same length and converge in a beam-combiner where they recombine to cause interference. This is known as a balanced MZI. To take advantage of phase variations and cause different interference patterns, we can add variations in the length of the paths, creating an unbalanced MZI. Additionally, thermo-optical phase shifters can be used to modify the effective index (n) or attenuation constants (α). With this structure in mind and assuming an input intensity I_i , with an electric field, E_i, the light is split equally into the two branches. Each branch has intensity $I_1 = I_2 = I_i/2$ and electric field $E_1 = E_2 = E_i/\sqrt{2}$

In the case of the electrical field E considering the propagation between the two y-branches the electrical field at the input of the beam combiner in the lossless case can be described by:

$$E_{o1} = E_1 e^{-i\beta_1} = \frac{E_i}{\sqrt{2}} e^{-i\beta L_1} \quad (1)$$

$$E_{o2} = E_2 e^{-i\beta L_2} = \frac{E_i}{\sqrt{2}} e^{-i\beta L_2} \quad (2)$$

Resulting in the beam combiner output:

$$E_o = \frac{1}{\sqrt{2}}(E_{o1} + E_{o2}) = \frac{E_i}{2}(e^{-i\beta L_1} + e^{-i\beta L_2}) \quad (3)$$

Where the propagation constant $\beta = \frac{2\pi n}{\lambda}$ and n is the index of refraction.

In the case of intensity at the output of the beam combiner for the lossless case we can describe it as:

$$E_o = \frac{I_i}{4}|e^{-i\beta L_1} + e^{-i\beta L_2}|^2 = \frac{I_i}{2}[1 + \cos(\beta \Delta L)] \quad (4)$$

Where $\Delta L = |L_1 - L_2|$ is the optical path length difference. By normalizing the output intensity to the input, assuming a lossless system, the transfer function for the unbalanced UMZI can be described as:

$$T_{MZI}(\lambda) = \frac{1}{2}[1 + \cos(\beta \Delta L)] \quad (5)$$

Lastly the free spectral range (FSR) of the interferometer can be described as:

$$FSR = \frac{\lambda^2}{(\Delta L n_g)} \quad (6)$$

Were n_g, the group index is described as:

$$n_g = n_{eff} - \lambda \frac{d_{neff}}{d_\lambda} \quad (7)$$

$$n_g = \frac{\lambda^2}{(\Delta L FSR)} \quad (8)$$

III. MODELLING AND SIMULATION

For the waveguide used in these interferometers a strip waveguide with a cross-section of 500nm width and 220nm height has been used. The 500 nm width has been chosen for convenience since it has been the standard studied so far in the course and the 220 nm height has been chosen due to the fabrication process used and its extensive use in the industry.

We can find in Table 1 the effective index of the fundamental TE and TM modes, calculated with Lumerical MODE. Figure 1 and Figure 2 contain results of the simulations of the electrical field intensity for both modes

working with a wavelength of 1500nm. In practice, all Mach-Zehnder interferometers of this document will be focused on quasi-TE polarization.

Mode	Effective index (neff)
TE1	2.4432
TM1	1.7639

Table 1. Effective index of TE and TM at 1550nm simulated strip waveguide

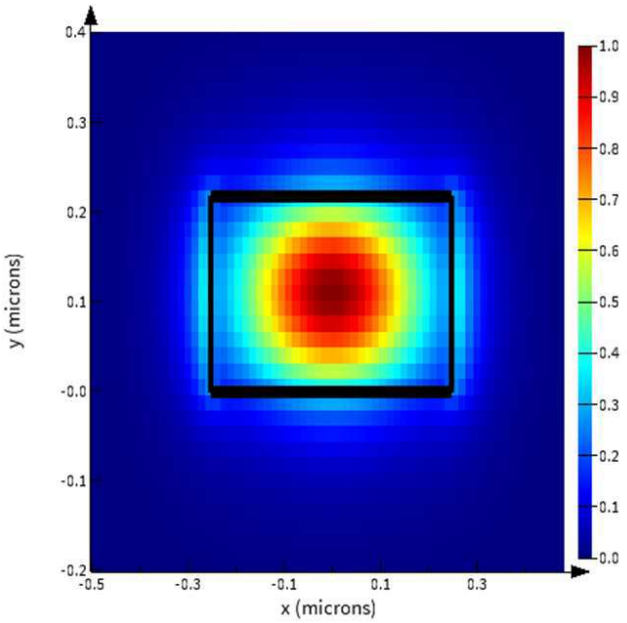

Fig 1. Electric field intensity of TE mode in the waveguide

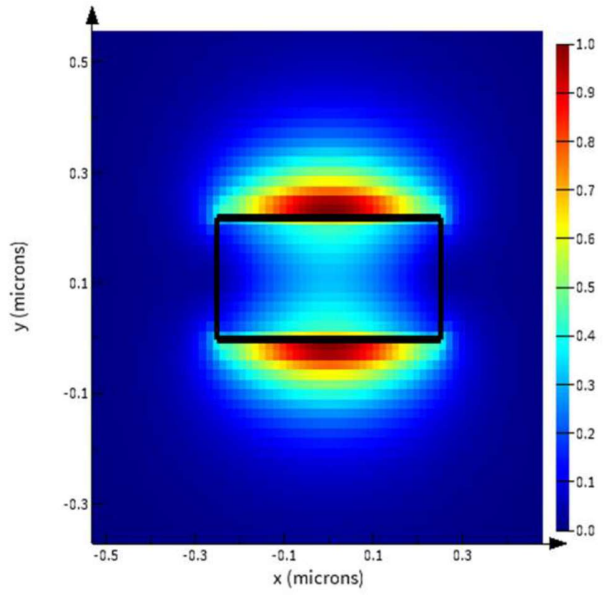

Fig 2. Electric field intensity of TM mode in the waveguide

Once the modes are calculated we can continue with a wavelength sweep of the waveguide between 1500 nm and 1600 nm to determine the variation of the effective and group index with reference to the wavelength. Figure 3 shows the variation of the effective index of the waveguide and Figure 4 shows the variation of the group index. As we can see, increasing the wavelength causes an increase in the group index and a reduction in the effective index.

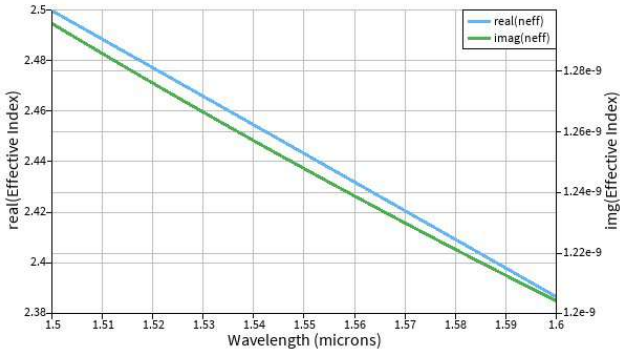

Fig 3. Variation of the effective index in reference to wavelength

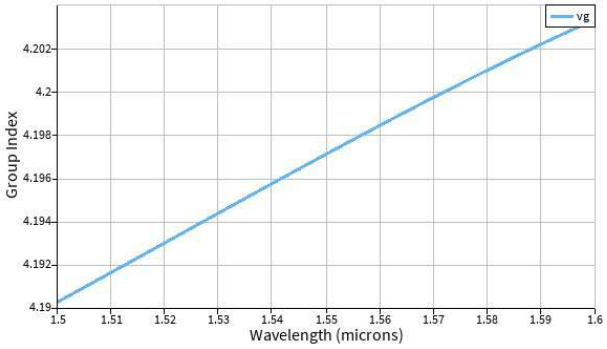

Fig 4. Variation of the group index in reference to Wavelength

From these sweeps and using the code script provided for the Lumerical MODE script prompt we can extract the values used for the compact waveguide model polynomial expression, resulting in the following expression that can be seen in Figure 5:

$$n_{eff}(\lambda) = 2.4432 - 1.1314(\lambda - 1.55) - 0.0427(\lambda - 1.55)^2 \quad (9)$$

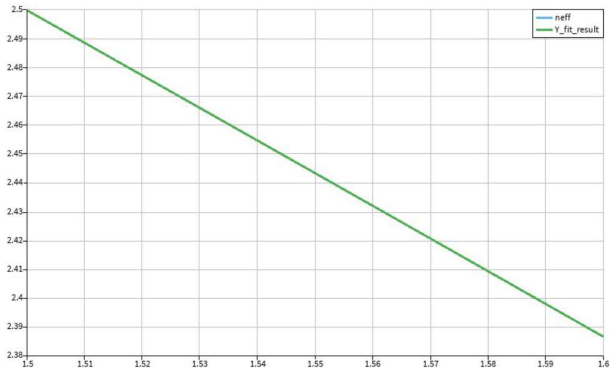

Fig 5. Polynomial fit for the compact waveguide

The variations of the interferometers will be focused on changes in the length between the two arms of the interferometer. There will be 5 variations with 25 micron increments between them, also an MZI with ΔL = 0 has been added for comparison purposes. Table 2 contains the different ΔL variations and the expected FSR using the mathematical expressions (5) and (6) for a wavelength of 1500nm.

ΔL (μm)	FSR (nm)
25	22.9
50	11.45
75	7.63
100	5.72
125	4.58

Table 2. Relation between distance variation and FSR at wavelength of 1550nm

For the simulation of the MZI in Lumerical interconnect, grating couplers, y branches and waveguides have been used. The grating couplers and y-branches are provided by the, course; the insertion losses can be seen in Figure 6 for one grating coupler and the transfer function for the y-branch in Figure 7. For the waveguides the parameters have been added using the results of the simulations done previously in Lumerical Mode.

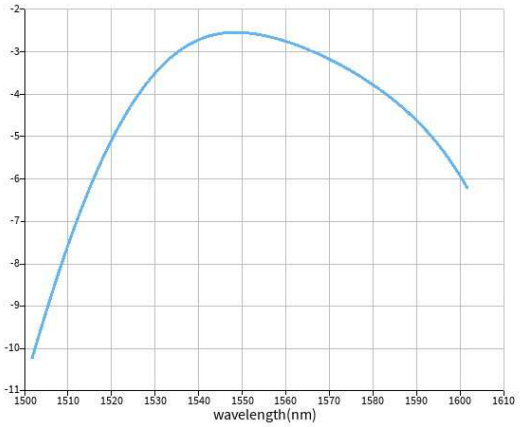

Fig 6. Grating coupler insertion loss (y axis - dB)

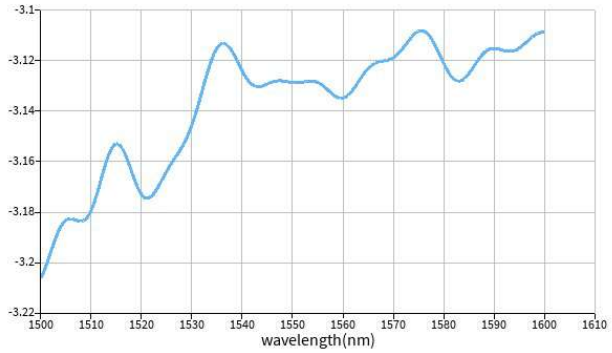

Fig 7. Y-branch transfer function (y axis - dB)

In Figure 8 the spectrum of 4 different MZIs with ΔL =0, 25, 75 um can be seen, note that these results, and the ones shown on Figure 9, are also affected by the mentioned grating couplers and y-branches.

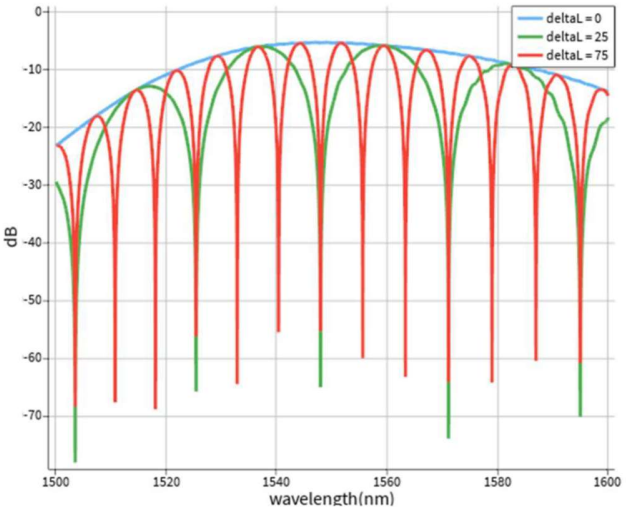

Fig 8. MZI spectrum with ΔL =0, 25, 75

Figure 9 shows the transmission of an MZI with ΔL =75.

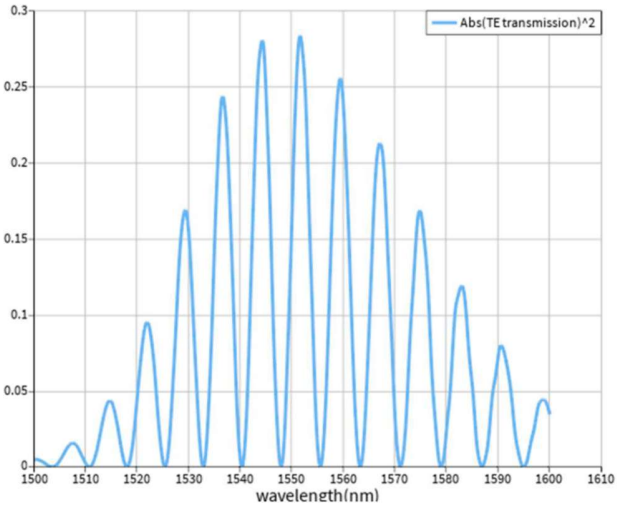

Fig 9. MZI transmission with ΔL = 75

IV. FABRICATION

The photonic devices were fabricated using the NanoSOI MPW fabrication process by Applied Nanotools Inc. (http://www.appliednt.com/nanosoi; Edmonton, Canada) which is based on direct-write 100 keV electron beam lithography technology [1]. Silicon-on-insulator wafers of 200 mm diameter, 220 nm device thickness and 2 µm buffer oxide thickness are used as the base material for the fabrication. The wafer was pre-diced into square substrates with dimensions of 25x25 mm, and lines were scribed into the substrate backsides to facilitate easy separation into smaller chips once fabrication was complete. After an initial wafer clean using piranha solution (3:1 H2SO4:H2O2) for 15 minutes and water/IPA rinse, hydrogen silsesquioxane (HSQ) resist was spin-coated onto the substrate and heated to evaporate the solvent. The photonic devices were patterned using a JEOL JBX-8100FS electron beam instrument at The University of British Columbia. The exposure dosage of the design was corrected for proximity effects that result from the backscatter of electrons from exposure of nearby features. Shape writing order was optimized for efficient patterning and minimal beam drift. After the e-beam exposure and subsequent development with a tetramethylammonium sulfate (TMAH) solution, the devices were inspected optically for residues and/or defects. The chips were then mounted on a 4" handle wafer and underwent an anisotropic ICP-RIE etch process using chlorine after qualification of the etch rate. The resist was removed from the surface of the devices using a 10:1 buffer oxide wet etch, and the devices were inspected using a scanning electron microscope (SEM) to verify patterning and etch quality. A 2.2 µm oxide cladding was deposited using a plasma-enhanced chemical vapour deposition (PECVD) process based on tetraethyl orthosilicate (TEOS) at 300ºC. Reflectrometry measurements were performed throughout the process to verify the device layer, buffer oxide and cladding thicknesses before delivery.

The fabrication design can present variabilities in the process of fabrication, between different wafers, chips on the same wafer and components on the same chip. We will focus on two of the more important variations that can occur, the width and height variation of our waveguides.

To account for the possible variations that can take place in the fabrication we use the Corner Analysis method, this allows us to represent the expected ranges for the performance of our designs. In our case the wafers are specified to be 219.2 nanometers in height plus or minus 3.9 nanometers, and in the case of waveguide width we use an interval from -30 to 10 nanometers.

We use four corners for analysis and a nominal variation:

- upper left (ul = 470*223.1 nm)
- upper right (ur = 510*223.1 nm)
- lower right (lr = 510*215.3 nm)
- lower left (ll = 470*215.3 nm)
- nominal (st = 500*219.2 nm)

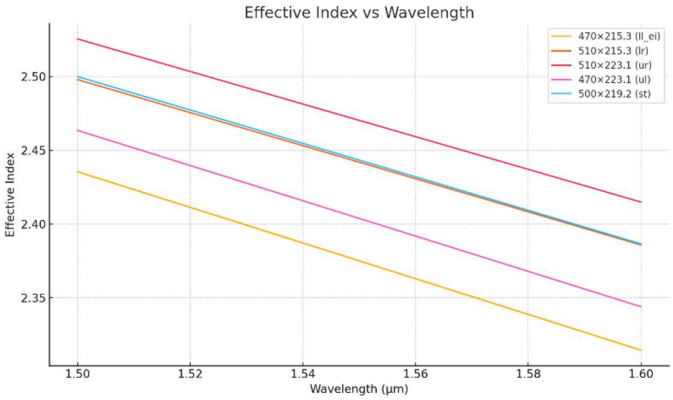

Fig 10. Effective index versus wavelength

In figure 10 we can see the variations of the effective index with each of the corners plus the nominal design in reference to the wavelength. As we can see there is a range of almost 0.1 variation in the effective index in the simulated waveguides depending on the fabrication variations. For figure 11 we see the group index with a range of 0.07 variations at the same wavelength. At a wavelength of 1550 nm we have a maximum of 4.255 and a minimum of 4.178 for the group index.

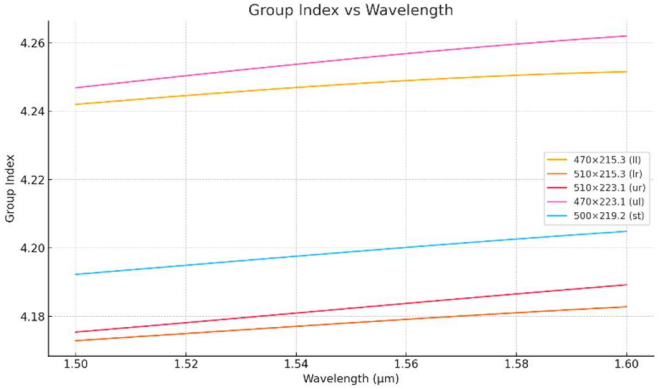

Fig 11. Group index versus wavelength

We can extract the various compact models for each of the waveguides.

- Upper left (10)
- Upper right (11)
- Lower right (12)
- Lower left (13)
- Nominal (14)

$$2.4038 - 1.1943(\lambda - 1.55) - 0.0497(\lambda - 1.55)^2 \text{ (10)}$$

$$2.4701 - 1.1046(\lambda - 1.55) - 0.0451(\lambda - 1.55)^2 \text{ (11)}$$

$$2.4418 - 1.1200(\lambda - 1.55) - 0.0325(\lambda - 1.55)^2 \text{ (12)}$$

$$2.3750 - 1.1325(\lambda - 1.55) - 0.0318(\lambda - 1.55)^2 \text{ (13)}$$

$$2.4432 - 1.1314(\lambda - 1.55) - 0.0412(\lambda - 1.55)^2 \text{ (14)}$$

And the transfer function and FSR for the UMZIs. A length variation of 100 (figures 12 and 13) and 50 (figures 14 and 15) microns has been chosen.

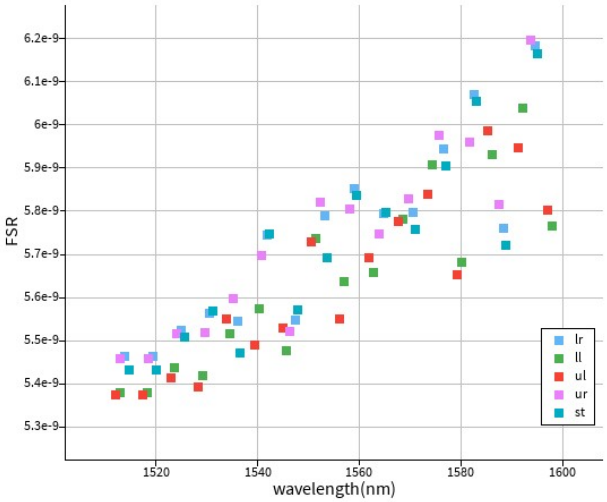

Fig 12. FSR UMZI Delta L 100

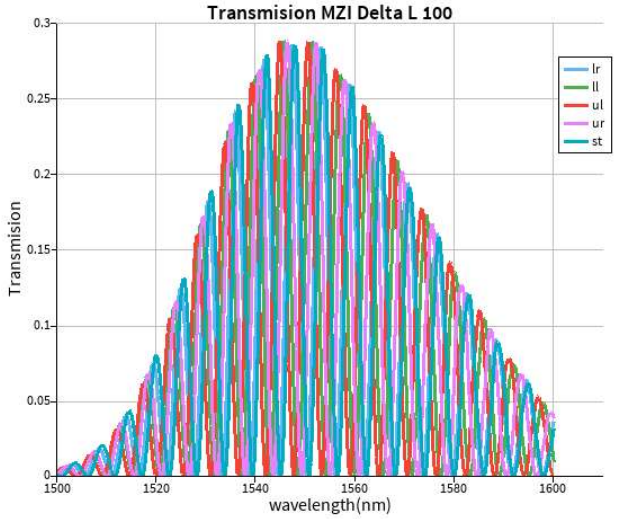

Fig 13. Transmission UMZI Delta L 100

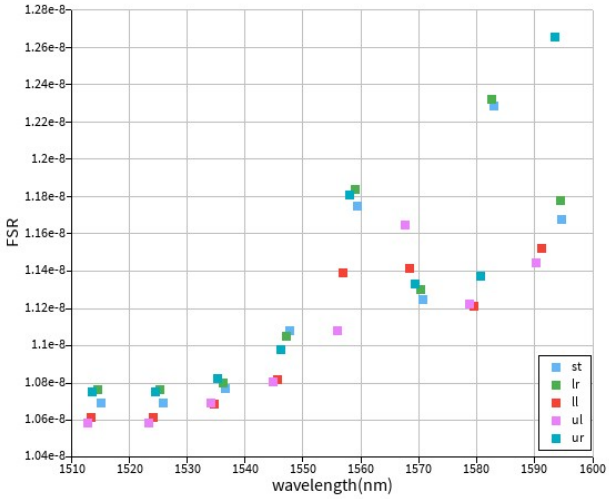

Fig 14. FSR UMZI Delta L 50

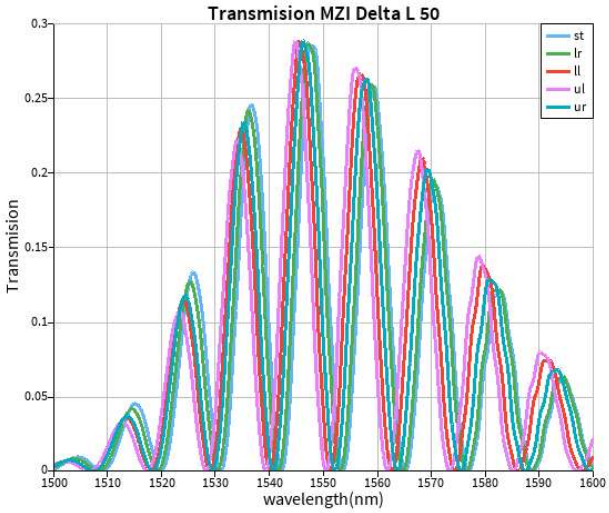

Fig 15. Transmission UMZI Delta L 50

The layout to be fabricated has been designed using Klayout and the PDK for the Ebeam process provided by the course. Represented in figure 16 we can find 5 UMZIs, 1 balanced MZI, a loop structure and 1 y-branch.

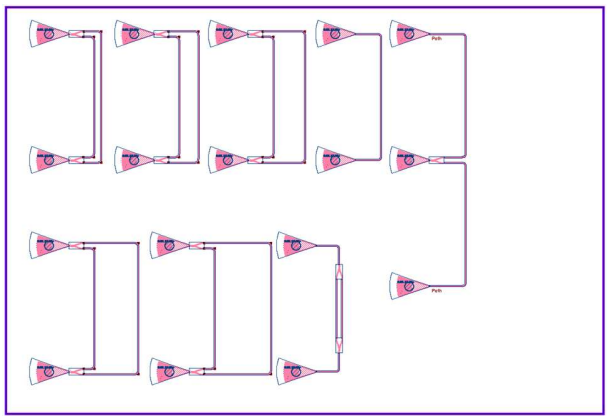

Fig 16. Layout submitted for fabrication

V. EXPERIMENT DATA & ANALYSIS

To characterize the devices, a custom-built automated test setup [2, 6] with automated control software written in Python was used [3]. An Agilent 81600B tunable laser was used as the input source and Agilent 81635A optical power sensors as the output detectors. The wavelength was swept from 1500 to 1600 nm in 10 pm steps. A polarization maintaining (PM) fiber was used to maintain the polarization state of the light, to couple the TE polarization into the grating couplers [4]. A 90º rotation was used to inject light into the TM grating couplers [4]. A polarization maintaining fiber array was used to couple light in/out of the chip [5].

The first problem that appears when measuring and analyzing the data extracted from the chip is the limited bandwidth of the grating couplers. In figure 17 we can see the spectrum of the two grating couplers (loop in layout), this curved spectrum will impact data from the measurements, as seen in figure 18, so the first step is to apply a baseline correction.

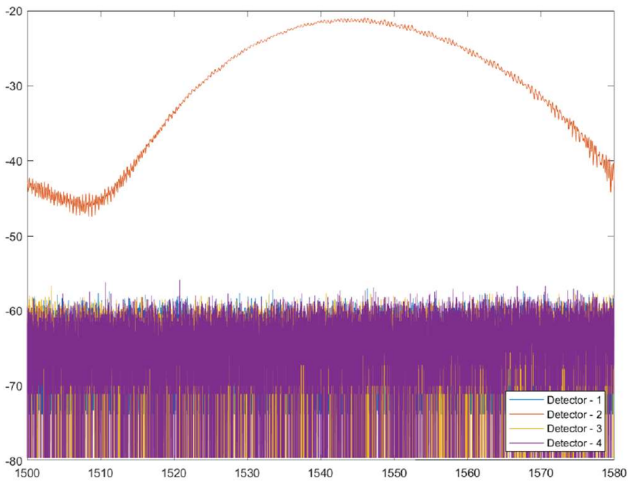

Fig 17. Grating couplers loop

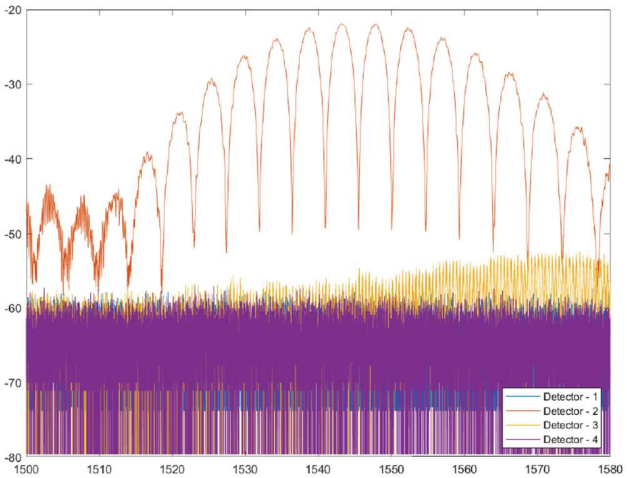

Fig 18. UMZI measurements (Delta L = 125)

For this we use the code provided for MATLAB scanning the range between 1515 nm and 1570 nm wavelengths. After this we have the result seen in figure 19, where we can see that the curve has been flattened.

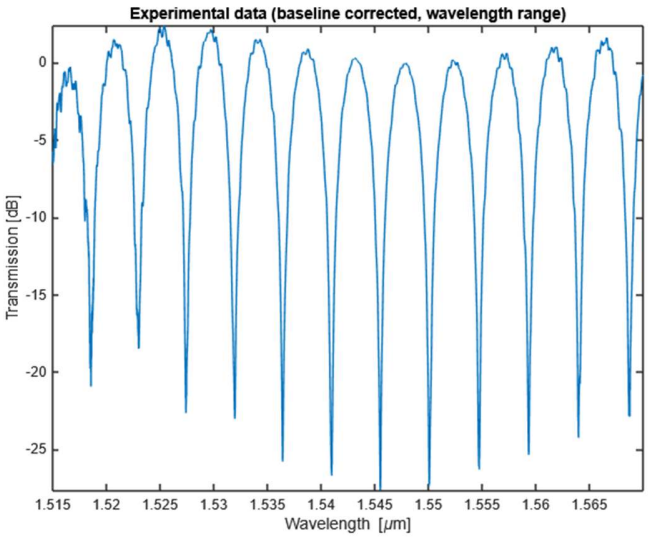

Fig 19. UMZI measurements (Delta L = 125)

The next step consists of matching our interferometer model to the experimental data, with the objective of extracting the waveguide parameters like the ones obtained previously in the simulations, mainly in the range simulated by the corner analysis. In this paper the method for fitting the MZI is the autocorrelation method. This method is based on estimating the periodicity of the spectrum (figure 20) using autocorrelation. From this periodicity we can then find the group index and the interferometer transfer function. We compare the transfer function to the experimental data and find a shift between the two data sets (figure 21). We adjust this by changing the effective index so that the simulations match cross correlating the simulation versus the experimental data assuming dispersion 0 (figure 22).

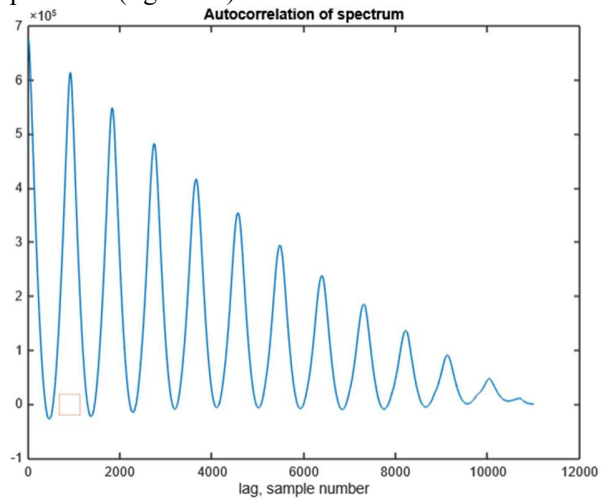

Fig 20. UMZI autocorrelation spectrum (Delta L = 125)

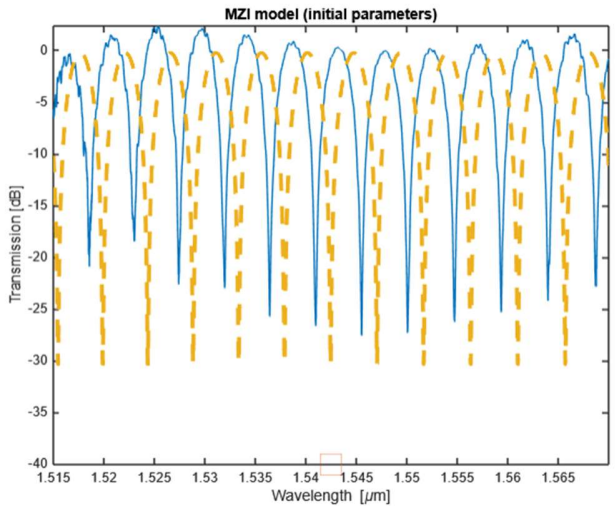

Fig 21. UMZI model initial parameters (Delta L = 125)

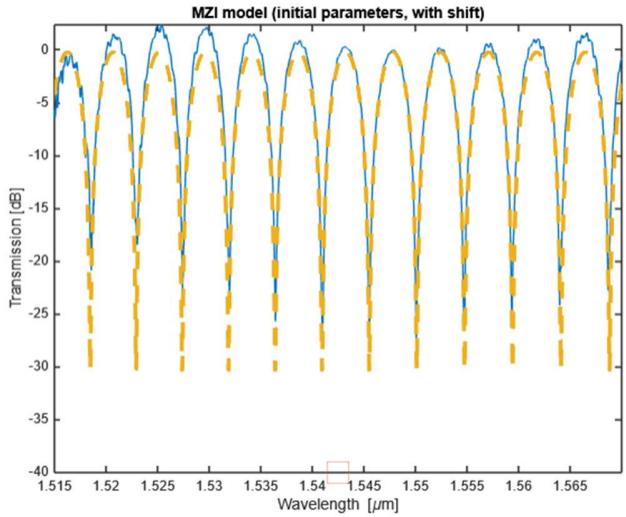

Fig 22. UMZI model parameters with shift (Delta L = 125)

Once this is achieved, we have the fit parameters for the MZI model (figure 23) and we can extract the waveguide parameters, namely the group index for this paper (figure 24).

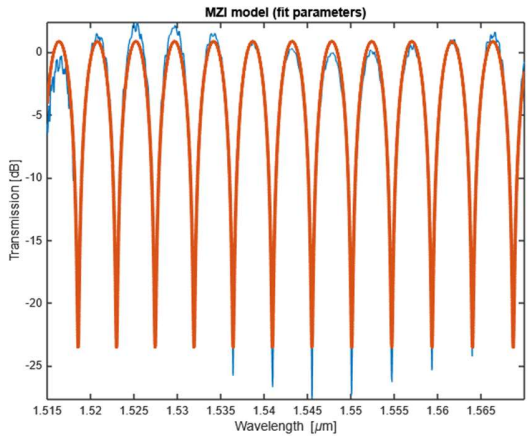

Fig 23. UMZI model fit parameters (Delta L = 125)

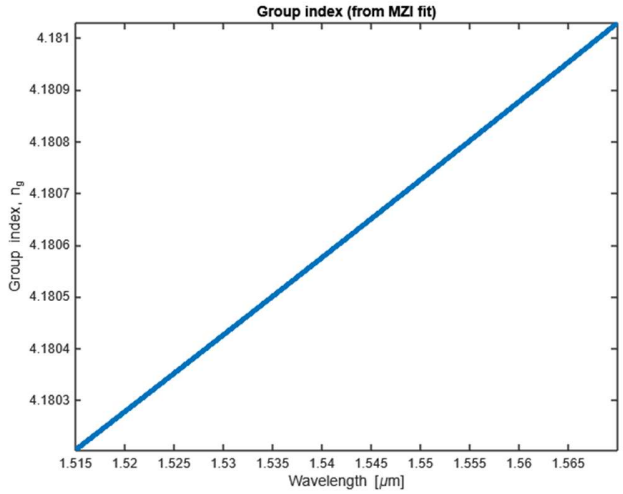

Fig 24. Waveguide group index (Delta L = 125)

VI. CONCLUSION

As we can see the group index is between the expected results for the corner analysis, in this case for a wavelength of 1550 nm the group index is 4.1806 which is inside the range calculated in the fabrication section.

VII. ACKNOWLEDGMENTS

I acknowledge the edX UBCx Phot1x Silicon Photonics Design, Fabrication and Data Analysis course, which is supported by the Natural Sciences and Engineering Research Council of Canada (NSERC) Silicon Electronic-Photonic Integrated Circuits (SiEPIC) Program. The devices were fabricated by Richard Bojko at the University of Washington Nanofabrication Facility, part of the National Science Foundation's National Nanotechnology Infrastructure Network (NNIN), and Cameron Horvath at Applied Nanotools, Inc. Omid Esmaeeli performed the measurements at The University of British Columbia. We acknowledge Lumerical Solutions, Inc., Mathworks, Mentor Graphics, Python, and KLayout for the design software.

VIII. REFERENCES

[1] R. J. Bojko, J. Li, L. He, T. Baehr-Jones, M. Hochberg, and Y. Aida, "Electron beam lithography writing strategies for low loss, high confinement silicon optical waveguides," J. Vacuum Sci. Technol. B 29, 06F309 (2011)

[2] Lukas Chrostowski, Michael Hochberg, chapter 12 in "Silicon Photonics Design: From Devices to Systems", Cambridge University Press, 2015

[3] http://siepic.ubc.ca/probestation, using Python code developed by Michael Caverley.

[4] Yun Wang, Xu Wang, Jonas Flueckiger, Han Yun, Wei Shi, Richard Bojko, Nicolas A. F. Jaeger, Lukas Chrostowski, "Focusing sub-wavelength grating couplers with low back reflections for rapid prototyping of silicon photonic circuits", Optics Express Vol. 22, Issue 17, pp. 20652-20662 (2014) doi: 10.1364/OE.22.020652

[5] www.plcconnections.com, PLC Connections, Columbus OH, USA.

[6] http://mapleleafphotonics.com, Maple Leaf Photonics, Seattle WA, USA.